

RESEARCH

Open Access



# Design and optimization of DPC-crosslinked HP $\beta$ CD nanosponges for entrectinib oral delivery: formulation, characterization, and pharmacokinetic studies

Konda Sri Chaya Reddy<sup>1</sup> and Darna Bhikshapathi<sup>1,2\*</sup>

## Abstract

**Background** In advanced or metastatic cancers characterized by specific genetic alterations, heightened growth and resistance to conventional therapies are common. Targeted treatments like entrectinib (ENT) precisely inhibit aberrant signaling pathways, potentially enhancing outcomes. The objective of this research is to develop and enhance the effectiveness of entrectinib-loaded nanosponge formulations by utilizing hydroxypropyl- $\beta$ -cyclodextrin (HP $\beta$ CD) to improve its oral bioavailability.

**Results** The study employed surface response methodology and Design-Expert<sup>®</sup> software to optimize key formulation variables such as the molar concentration ratio of the polymer and cross-linker, as well as process variables such as stirring speed and duration. Optimization focused on particle size, polydispersity index, and percentage entrapment efficiency. Validation methods encompassed Fourier transform spectroscopy (FTIR), differential scanning calorimetry (DSC), scanning electron microscopy (SEM), in vitro release studies, and in vivo studies.

After optimization, ENT-loaded HP $\beta$ CD NSPs were formulated with a molar ratio (P:CL) of 0.800 mg, stirred at 3000 rpm for 420 min, achieving a desirability of 0.926. Predicted values for PS (particle size), PDI (polydispersity index), and EE % (entrapment efficiency) were 146.98 nm, 0.263, and 88.29%, respectively. The optimized formulation showed a mean size of  $151.8 \pm 5.6$  nm, PDI of  $0.233 \pm 0.049$ , and EE of  $87.36 \pm 1.61\%$ . Further validation through various analyses confirmed the optimization's efficacy, with notable improvements demonstrated in AUC<sub>0-t</sub> (6.30-fold) and C<sub>max</sub> (4.10 times) compared to the free drug.

**Conclusion** The findings of the study indicated that nanosponges exhibit promise as an effective carrier for delivering entrectinib, addressing for advance tumor effectively by enhancing release and bioavailability in the treatment of cancer.

## Highlights

- Entrectinib (ENT) is an innovative and powerful inhibitor targeting specific genetic alterations in advanced or metastatic cancers.

\*Correspondence:

Darna Bhikshapathi  
dbpathi71@gmail.com

Full list of author information is available at the end of the article



© The Author(s) 2024. **Open Access** This article is licensed under a Creative Commons Attribution 4.0 International License, which permits use, sharing, adaptation, distribution and reproduction in any medium or format, as long as you give appropriate credit to the original author(s) and the source, provide a link to the Creative Commons licence, and indicate if changes were made. The images or other third party material in this article are included in the article's Creative Commons licence, unless indicated otherwise in a credit line to the material. If material is not included in the article's Creative Commons licence and your intended use is not permitted by statutory regulation or exceeds the permitted use, you will need to obtain permission directly from the copyright holder. To view a copy of this licence, visit <http://creativecommons.org/licenses/by/4.0/>.

- Preclinical investigations have shown strong suppression of receptor tyrosine kinases, such as TRKA/B/C and ROS1, at nanomolar (nM) concentrations using ENT.
- ENT is categorized under the Biopharmaceutical Classification Systems (BCS) II, with poor solubility and inadequate oral bioavailability.
- Formulation of ENT HP $\beta$ CD based nanosponges (NSPs) present a compelling option for drug delivery due to their sustained drug release, enhanced stability, and significant carrying capacity.

**Keywords** Box–Behnken design, Cross-linker, Hydroxypropyl- $\beta$ -cyclodextrin, Solubility, Entrectinib, Diphenyl carbonate, Quality by design

## Introduction

Entrectinib (ENT) is an innovative and powerful inhibitor targeting tyrosine receptor kinases (TRKA, TRKB, and TRKC), ROS1, and anaplastic lymphoma kinase (ALK) with oral administration capabilities [1]. In 2019, approval was granted in Japan for an emerging therapy aimed at meeting the requirements of pediatric and adult patients with neurotrophic tropomyosin receptor kinase (NTRK) fusion-positive advanced or solid tumors. Both the FDA and the European Union have sanctioned this therapy for the treatment of solid tumors and non-small cell lung cancer (NSCLC). Additionally, it has shown efficacy in the treatment of brain metastases [2].

Preclinical studies demonstrate ENT's potent suppression of TRKA/B/C and ROS1 receptor tyrosine kinases at nanomolar concentrations. Notably, ENT effectively combats aggressive solid brain tumors by traversing the blood–brain barrier, hindering tumor progression [3, 4].

Entrectinib (ENT) is classified as a BCS II drug due to its poor solubility (0.0089 mg/mL) and high log p-value of 5.03. Despite being effective against non-small cell lung cancer (NSCLC), ENT has limited oral bioavailability due to significant protein binding and extensive first-pass metabolism. Additionally, its solubility is pH-dependent, with solubility levels exceeding 40 mg/mL at pH 1.2, but dropping significantly to 0.03 mg/mL and 0.002 mg/mL at pH 5.4 and 6.4, respectively [5, 6]. ENT exhibits greater solubility postprandially than during fasting [7].

Recommended adult and pediatric doses are 600 mg and 400 mg, respectively, but higher doses may cause severe side effects [8]. ENT's interactions with other medications are well-documented. Controlling drug release through formulation strategies can mitigate side effects. Addressing pharmacokinetic variability and the first-pass effect linked to the current capsule formulation is crucial [9].

Nanotechnology adoption is crucial in such scenarios, offering innovative solutions. Colloidal nanocarriers for drug delivery help overcome traditional method limitations. SNEDDS enhance solubility, addressing these challenges effectively [10]. In our previous work, we have reported nanosponges of ENT using beta-cyclodextrins ( $\beta$ CD) but we did not report the *in vivo* studies [11]. The shift from beta-cyclodextrins ( $\beta$ CD) to hydroxypropyl-beta-cyclodextrins (HP $\beta$ CD) in pharmaceutical formulations is driven by significant adverse effects associated with  $\beta$ CD. HP $\beta$ CD offers enhanced safety profiles, leading to its widespread adoption in numerous marketed products. Its lower propensity for adverse reactions, including nephrotoxicity, makes HP $\beta$ CD a preferred choice for drug delivery systems and formulations [12].

Given the commercial potential of HP $\beta$ CD, our study explores strategies to enhance solubility, sustainability, and bioavailability by modulating pharmacokinetic profiles [13]. Nanosponges, known for their colloidal size and nanoscale voids, present a potential solution for drug encapsulation and controlled release. By utilizing HP $\beta$ CD, nanosponges improve pharmaceutical formulations, providing sustained drug release, stability, a large carrying capacity, and the ability to encapsulate various molecules [14, 15]. Safe formulations that target specific locations and enable gradual drug release are vital to minimize toxicity and nonspecific distribution. The production of nanosponge particles (NSPs) is simple, scalable, and cost-effective. Transforming pharmaceuticals into nanoscale sponges presents a sensible solution, considering its numerous benefits. The aim was to enhance ENT bioavailability through HP $\beta$ CD nanosponges (NSPs), regulating delivery to target locations. Factors affecting process and formulation were investigated to optimize NSPs. Analysis techniques such as DSC, SEM, FTIR, and XRD were employed on the optimized formulation. *In vitro* release and pharmacokinetic experiments

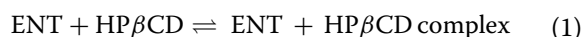
assessed bioavailability enhancement. HP $\beta$ CD nanosponges effectively serve as ENT carriers, enabling gradual release over an extended period.

## Materials

Entrectinib pure drug was acquired from Hetero Drugs Ltd., Hyderabad, India. Sigma-Aldrich, US, supplied hydroxypropyl- $\beta$ -cyclodextrin (HP $\beta$ CD), diphenyl carbonate (DPC), and glutaraldehyde (25% aqueous solution). Solvents were acquired from S.D. Fine Chemicals, Hyderabad. HiMedia Pvt. Ltd. supplied the dialysis membrane (cutoff of MWt. 12 kDa).

## Phase solubility study

Solubility analysis followed the Higuchi and Connors protocol. HP $\beta$ CD aqueous solutions ranging from 0 to 40 mM were prepared with excess ENT in vials. Stirring at room temperature for 72 h in the dark was done using a magnetic stirrer. Supernatants were subjected to centrifugation at a speed of 15,000 rpm for a duration of 30 min at a temperature of 4 °C. Following this, the ENT concentration was quantified by analyzing the supernatants using a PerkinElmer Lambda 25 UV spectrophotometer at a wavelength of 262 nm. Mean values  $\pm$  standard deviation was reported after three repetitions. Solubility profiles were created by plotting ENT concentration (mM) against HP $\beta$ CD concentration (mM). Equation (2) was used to determine the stability constant (K1:1) from the solubility-phase profile slope, assuming 1:1 complex formation between ENT and HP $\beta$ CD.



$$K1 : 1 = \frac{[\text{ENT} \cdot \text{HP}\beta\text{CD complex}]}{[\text{ENT}] X [\text{HP}\beta\text{CD}]} \quad (2)$$

$$= \frac{\text{slope}}{\text{ENT}_0} \times (1 - \text{slope})$$

ENT<sub>0</sub>: intrinsic solubility of ENT in ultrapure water; [ENT.HP $\beta$ CD complex] denotes the concentration of dissolved composite,

[HP $\beta$ CD] suggests the concentration of free HP $\beta$ CD in the aqueous complexing media.

## Preparation of the ENT/HP $\beta$ CD complex

ENT/HP $\beta$ CD complexes were prepared by combining equal amounts of the drug and HP $\beta$ CD in 1 mL of methanol and distilled water, following the established procedure [16].

## Production of HP $\beta$ CD-based nanosponges

The nanosponges (NSPs) made from HP $\beta$ CD were constructed by combining HP $\beta$ CD and DPC in a ratio of 1:6. DPC was used as the cross-linking agent during the synthesis process. Ultrasound-assisted technique was employed following previous protocols with minor adjustments [17]. HP $\beta$ CD was dissolved in dimethylformamide in a 250-mL flask, followed by addition of DPC. The reaction mix was refluxed at 90 °C in an oil bath until liquefied. The resulting product underwent purification by Soxhlet extraction with ethanol, water wash, and overnight drying at 60 °C.

The dried material was finely powdered and then mixed with water and subjected to lyophilization for long-term stability. For formulating ENT-HP $\beta$ CD NSPs, dispersion of HP $\beta$ CD in distilled water was followed by addition of the drug and probe sonication. Continuous stirring and sonication were performed, followed by centrifugation to separate uncomplexed drug. The supernatant was freeze-dried, yielding a dry mass preserved in a desiccator.

## Experimental design

Seventeen formulations were created using Design-Expert software version 13.0 by Stat-Ease Inc. in Minneapolis, MN, USA. A three-factor three-level experimental design was employed with independent variables: molar

**Table 1** Components of experimental design

	Independent variables	Levels		
		Low (-1)	Medium (0)	High (+1)
A	Molar ratio of P:CL (mg)	0.4	0.6	0.8
B	Stirring speed (rpm)	2000	4000	6000
C	Stirring duration (mins)	240	330	420
Responses		Constraints		
X	Particle size	Minimize		
Y	PdI	Minimize		
Z	EE	Maximize		

ratio of P:CL (A), stirring speed (B rpm), and stirring duration (C mins). Dependent variables, including particle size (X), PDI (Y), and entrapment efficiency (Z), were evaluated (Table 1).

### HPLC analysis

#### Equipment

An undisturbed sustained Symmetry ODS C18 column (250×4.6 mm in diameter, 5-micron meter particle size), Shimadzu (Shimadzu Prominence pump model -LC-20AD) HPLC with UV/Visible indicator, was used to complete the chromatographic separation. The mobile phase consists of methanol and phosphate buffer (35:65) v/v. An isocratic mode at a 1 mL/min flow rate was used. After introducing 20 µL of samples, the eluents were examined at a wavelength of 235 nm.

#### Preparation of standards

The primary stock (1 mg/mL) was prepared by weighing ENT and carbamazepine (internal standard). Next, utilizing a secondary stock containing 100 µg/mL, a curve for calibration between 0.250 and 200 ng/mL was produced.

#### The extraction of a sample for bioanalysis

ENT was recovered from plasma samples via the protein precipitation method. The drug was successfully extracted from plasma by adding acetonitrile (250 µL) to rat plasma (50 µL) and vortexed. The supernatant was centrifuged for 10 min at 8500 rpm and then analyzed using chromatography at a  $\lambda_{max}$  of 235 nm.

### Evaluation and physicochemical characterization

#### Particle size (PS), polydispersity index (PDI), and zeta potential (ZP)

The HPβCD NSPs were analyzed for particle size (PS) and polydispersity index (PDI) using dynamic light scattering (DLS) on a Malvern Zetasizer (Malvern Instruments, UK). The samples underwent a tenfold dilution, followed by dispersion in double-distilled water, and were subsequently analyzed using a Zetasizer (Malvern) at a temperature of 25 °C. Each measurement was conducted three times, allowing for the calculation of particle size and PDI values [18].

#### Entrapment efficiency (EE) and yield percentage

The EE of drug in the nanosponges can influence the therapeutic efficacy, stability, and release kinetics of the loaded compounds within the nanosponges. Dichloromethane was used to dissolve a particular quantity of loaded drug (ENT)-containing nanosponges (NSPs). The complex was dissolved by subjecting the solution to sonication for 12 min. The resultant solution was then

suitably diluted and subjected to high-performance liquid chromatography analysis (HPLC). UV absorbance was used to detect the drug at a wavelength of 235 nm [19]. The drug-loaded nanosponges were weighed after complete drying. The following formulae were used to calculate the % EE and yield percentage.

$$\begin{aligned} \text{\% Drug Entrapment efficiency} \\ &= \frac{\text{Total amount of the drug} - \text{free drug}}{\text{amount of drug}} \times 100 \end{aligned}$$

$$\text{Yield percentage} = \frac{\text{Weight of Nanosponges}}{\text{Total solid weight}} \times 100$$

#### Morphology using scanning electron microscopy (SEM)

Using a Quanta FESEM 250 SEM, the structure of the nanosponges was captured. Before testing, the sample was mounted on aluminum pin stubs after being double-sided carbon tape-mounted and Au sputter coated utilizing an ion sputter. The specimen was then analyzed at an operating distance of 10 mm, with an acceleration current of 30 kV and a magnification of 500–10,000 folds [18].

#### Fourier transform infrared (FTIR) spectroscopy

The spectrum of FTIR was obtained using spectroscopy PerkinElmer (Model 1600; USA). The pure drug, physical mixture (PM), and the optimized drug-loaded HPβCD NSPs were all analyzed at wavenumbers 4000–450 cm<sup>-1</sup> with a resolution of 1.0 cm<sup>-1</sup> [11].

#### Differential scanning calorimetric study and X-ray diffraction pattern (XRD)

DSC (DSC-60, Shimadzu Corp., Japan) was employed to ascertain the drug's physical structure and the potential for chemical interactions with the excipients. Samples of 3–5 mg (drug, PM, and optimized drug-loaded HPβCD NSPs) were subjected to heating (50–400 °C, 5 °C/min) in folded aluminum pans in a nitrogen environment before being subjected to DSC analysis following calibration using indium and lead standards. The melting point (MP) and the enthalpy of fusion were computed automatically [20]. The X-ray diffraction patterns of pure drug, physical mixture, and the optimized formulations were obtained using a Philips X-ray diffract meter (PW-1710) equipped with a graphite monochromator and Ni-filtered Cu K $\alpha$  radiation. The scan was conducted at a speed of 1° 2 $\theta$  min<sup>-1</sup>, with a current of 20 mA and a voltage of 30 kV.

#### Drug release (DR)

The release studies of (PD) pure drug and optimized drug-loaded β-CD NSPs were carried out through

in vitro experiments using a shake flask equipped with a dialysis bag. Following encapsulation in dialysis membranes, the specimens were transferred into a conical flask containing phosphate buffer (pH 6.8), maintained at 37 °C, and subjected to constant rotation at 100 rpm. One milliliter sample was taken off from the outer solution and replaced with brand-new PBS at pH 6.8 at predefined intervals. These aliquots were filtered and analyzed at 235 nm using HPLC analysis to measure drug release. Three duplicates of the experiment were carried out. Several kinetic models were fitted to know the mechanism. The highest correlation coefficient ( $R^2$ ) was used to determine the most suitable model. The slope and  $R^2$  values were used to calculate the release-exponent value, representing the drug release mechanism.

#### Stability studies

The optimized formulation's stability was evaluated by storing at three temperatures (4 °C, 25 °C, and 40 °C) at a with 75% relative humidity. Regular intervals were set to measure particle size and PDI changes in the samples taken [21].

#### Pharmacokinetic studies (PKs)

The Nutrition National Institute (NIN), situated in Telangana, India, provided the male Wistar rats used in the study, which had an approximate weight of  $200 \pm 20$  g and an age of 4–5 weeks. The animal study followed the "Guidelines for Care and Use of Laboratory Animals", and the Institutional Animal Ethics Committee (IAEC) officially sanctioned the protocol designed by the protocol number 1447/PO/Re/S/11/CPCSEA-83/A. Animals were exposed to natural light/dark settings for 1 week, where they were acclimated to a relative humidity of 40–60% and a temperature of  $20 \text{ }^\circ\text{C} \pm 2 \text{ }^\circ\text{C}$ . After that, they were randomly divided into three groups of six animals. The optimized drug-loaded HP $\beta$ CD NSPs (30 mg/kg BW), the vehicle, and the pure drug (dispersed in 0.5% w/v sodium carboxy methylcellulose) were administered by oral route. Blood samples (200  $\mu$ L) were collected from the retro-orbital plexus and transferred into sterile test tubes containing EDTA at specific time intervals (0.25, 0.5, 1, 2, 4, 6, 12, and 24 h). The blood samples were then centrifuged at 7500 rpm for 10 min using an Eppendorf centrifuge. The resulting plasma was further analyzed using high-performance liquid chromatography (HPLC).

#### The extraction of a sample for bioanalysis

ENT was recovered from plasma samples via the protein precipitation method. The drug was successfully

extracted from plasma by adding acetonitrile (250  $\mu$ L) to rat plasma (50  $\mu$ L) and vortexed. The supernatant was centrifuged for 12 min at 8000 rpm and then analyzed using chromatography at a  $\lambda_{\text{max}}$  of 235 nm.

#### Data analysis

Data analysis was performed using WinNonlin (version 3.1; Pharsight et al. USA) on the acquired concentration–time profile. The pharmacokinetic variables were examined using the non-compartmental methodology.

#### Statistical analysis

The pharmacokinetic variables' standard deviation (SD) was represented as Mean  $\pm$ . The variables were further examined using GraphPad Prism's statistical analysis program (GraphPad Software 8.05 Inc., CA).

## Results

#### Phase solubility studies

The plot of the phase solubility study is depicted in Suppl. Figure 1. A 1:1 molar ratio inclusion complex (ENT:HP $\beta$ CD) is suggested by the slope value, which is less than 1 and the apparent stability constant,  $K_{1:1}$ , which was determined to be  $214.04 \text{ M}^{-1}$ , and the solubility was increased by 18-fold. The analysis revealed that the concentration of HP $\beta$ CD directly influences the solubilization of ENT in a linear fashion. This indicates that the concentrations of both ENT and HP $\beta$ CD decrease in a linear fashion when an ENT/HP $\beta$ CD solution is given, either through oral or intravenous administration, thereby reducing the chances of precipitation taking place [18].

#### Formulation of nanosponges

Nanosponges of ENT were created through the process of inclusion complexation, where hydroxypropyl-beta-cyclodextrins (HP $\beta$ CD) serve as host molecules, forming empty spaces within their structure to hold drug molecules, resulting in inclusion complexes. This formation is made possible by HP $\beta$ CD's capability to form hydrogen bonds with the drug molecules, enclosing them within their hydrophobic core [12]. Since lyophilization effectively increases stability, the NSPs were subjected to freeze-drying after the formation.

#### FbD-based approach

The objective of ENT-loaded HP $\beta$ CD NSPs was to improve bioavailability through sustained release. Consequently, a well-defined quality targeted product profile (QTPP) was established for the formulation and is outlined in Table 2.



**Table 2** QTPP and CQAs selection and justification

	Target	Justification
<i>QTPP</i>		
Formulation	Nanosponges (NSPs)	The NSPs of ENT will give provide sustain release of drug
Route of administration	Oral	The existing formulation is designed for oral administration, and our efforts are directed toward enhancing its oral bioavailability
Dissolution	Higher compared to plain drug	Sustained release at the target site could enhance the availability of the drug
Pharmacokinetics	It should be more effective than the currently available version	For increased bioavailability
Stability	The NSPs formulation lasts for up to 90 days with no obvious evidence of aggregation and large particle size	Maintaining the same particle size is crucial because the formulation's efficiency depends on it
<i>CQAs</i>		
Particle size	nm	When size is lowered to the nanoscale, more surface area is available, which promotes both release and dissolution. Dissolving and releasing energy slowly increases bioavailability
Pdl	Less than 0.3	Less Pdl is an indication of homogeneity of the formulation, and hence, it is kept as less than 0.3
EE	High	High entrapment helps to reduce the dose of the drug

**Table 3** Runs designed for the trails

Run	ENT amount	Factor 1	Factor 2	Factor 3	Response 1	Response 2	Response 3
		A: Molar ratio (P:CL) mg	B: Stirring speed RPM	C: Stirring duration Mins	PS nm	Pdl	EE %
1	60 mg	0.6	4000	330	176	0.32	71.7
2		0.4	3000	330	236.6	0.41	70.6
3		0.8	3000	330	154	0.261	85.3
4		0.6	3000	240	174	0.32	77.8
5		0.6	5000	420	268	0.34	77.9
6		0.4	5000	330	302.3	0.41	69.8
7		0.6	4000	330	206.5	0.278	75.8
8		0.6	5000	240	226	0.386	75.2
9		0.6	3000	420	222	0.32	80.4
10		0.8	4000	240	151.4	0.3	83.9
11		0.6	4000	330	182	0.34	79
12		0.8	4000	420	153	0.31	88.9
13		0.4	4000	240	246	0.38	65.8
14		0.4	4000	420	270	0.42	71.8
15		0.8	5000	330	156	0.228	86.3

### Experimental design

The study had fifteen runs, with three center locations (Table 3). Multiple linear regressions created polynomial models by considering linear, quadratic, and two-factor interaction (2FI) factors. The model selection (CV) was done using the coefficient of variance, adjusted  $R^2$ , and forecasted  $R^2$ .

### PS (particle size)

Initial screening revealed that the molar ratio of polymer to cross-linker, stirring speed, and stirring time significantly influenced mean particle size (PS), entrapment efficiency (% EE), and polydispersity index (Pdl) of ENT HP $\beta$ CD NSPs. These variables were individually investigated, establishing ranges of 0.2–0.8 for the molar ratio,

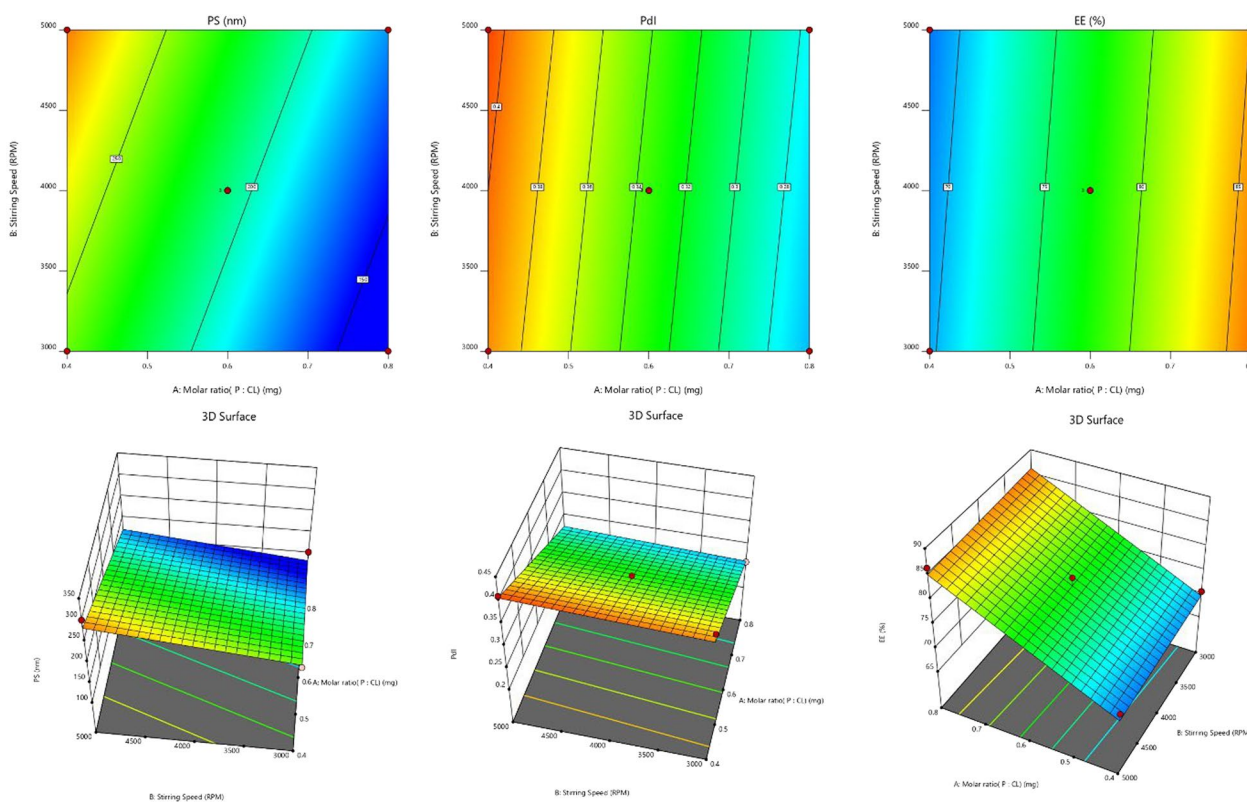


**Fig. 1** Response surface and contour plots illustrating variable effects on particle size PS, Pdl, and EE

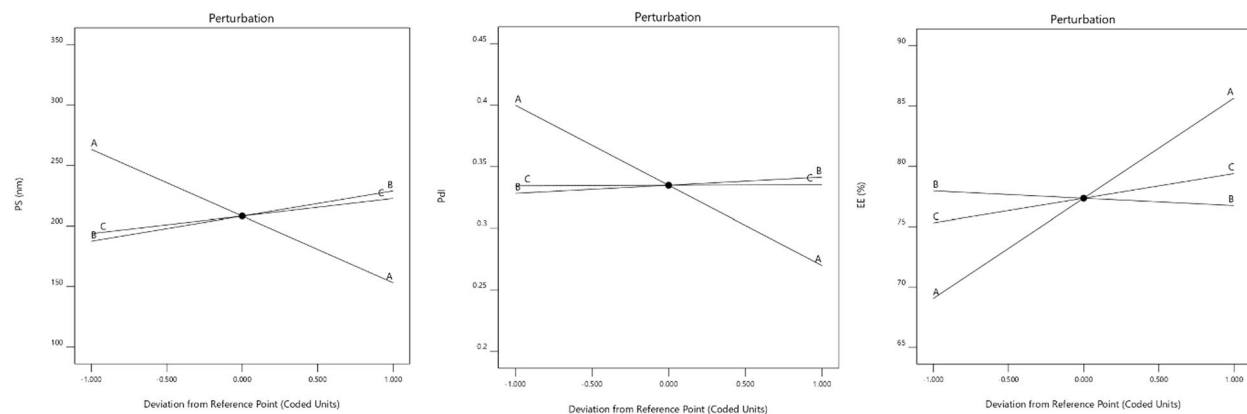


**Fig. 2** Graphical depiction of perturbation plot and effects variables on PS, Pdl, and EE

3000–5000 rpm for stirring speed, and 240–420 min for stirring time. PS ranged from 151.4 to 302.3 nm, Pdl from 0.228 to 0.42, and % EE from 65.8 to 88.9% across batches. A linear model fitted to responses, validated by Design-Expert software’s ANOVA tests, indicated significance with an insignificant lack of fit (1.68) and a model F-value of 24.10.  $R^2$ , adjusted  $R^2$ , and anticipated  $R^2$  were 0.8679, 0.8319, and 0.7681, respectively, demonstrating

sufficient precision (14.564) in exploring the design space.

With p-values of less than 0.05, all the typical relationships (A, B) significantly affected the outcome. These variables are now regarded as being meaningful, and the subsequent equation for regression is given as follows:

$$\text{Particlessize} = +208.25 - 55.06A + 20.71B + 14.45C$$

Three-dimensional response surface plots, contour plots, and perturbation functions were utilized to assess the primary and interacting effects of individual variables on particle size (PS). Figure 1 depicts the response surface and contour plots illustrating variable effects on PS. Additionally, Fig. 2 presents the perturbation plot (two-dimensional) demonstrating the effect of the molar ratio of polymer to cross-linker, stirring speed, and stirring duration on mean particle size, with a comparison between predicted and actual values. The increase in the molar ratio of cross-linker to polymer resulted in a decrease in particle size, with stirring speed (B) and stirring duration (C) showing less influence compared to variable A [11].

**PdI (polydispersity index)**

A dimensionless measure of the particle size distribution's broadness is the polydispersity index (PdI). Typically, it falls between 0 and 1 [22]. PdI ranging from 0.228 to 0.42 was observed in the developed formulations. The model *F*-value of 10.87 indicates a slight lack of fit for the suggested linear model, which was significant. Lack of fit, statistically insignificant based only on pure error, yielded an *F*-value of 1.06. ANOVA identified significant factors (*p*-value < 0.0500), with non-significant variables removed to refine the model.

Regression coefficient values ( $R^2$ , adjusted  $R^2$ , and anticipated  $R^2$ ) were 0.7477, 0.6789, and 0.5352, respectively. The model demonstrated utility in examining the design space, with an adequate precision of 8.5697, surpassing the necessary value of 4.

The model terms *A* were learned to have *p*-values less than 0.050, indicating a substantial impact on the outcome. Consequently, these terms are deemed necessary, and the resulting regression equation is as follows:

$$PDI = +0.3349 - 0.0651A + 0.0066B - 0.0005C$$

Positive coefficients indicate a positive correlation, suggesting that an increase in the associated variable leads to an increase in PdI. Conversely, negative coefficients (-0.0155) suggest a negative correlation, indicating that a decrease in the related variable results in a reduction in PdI. Response surface plots (Fig. 3) demonstrate that homogenization speed significantly influences PdI. Despite all formulations maintaining PdI within acceptable bounds, below 0.3, higher stirring speed of the polymer to cross-linker at a lower molar concentration led to a slight increase in PdI. Faster stirring initially enhances monodispersity, but excessive stirring imparts more energy to the particles, reducing their repulsive forces and causing agglomeration. This observation aligns with size expansion surpassing ideal homogenization.

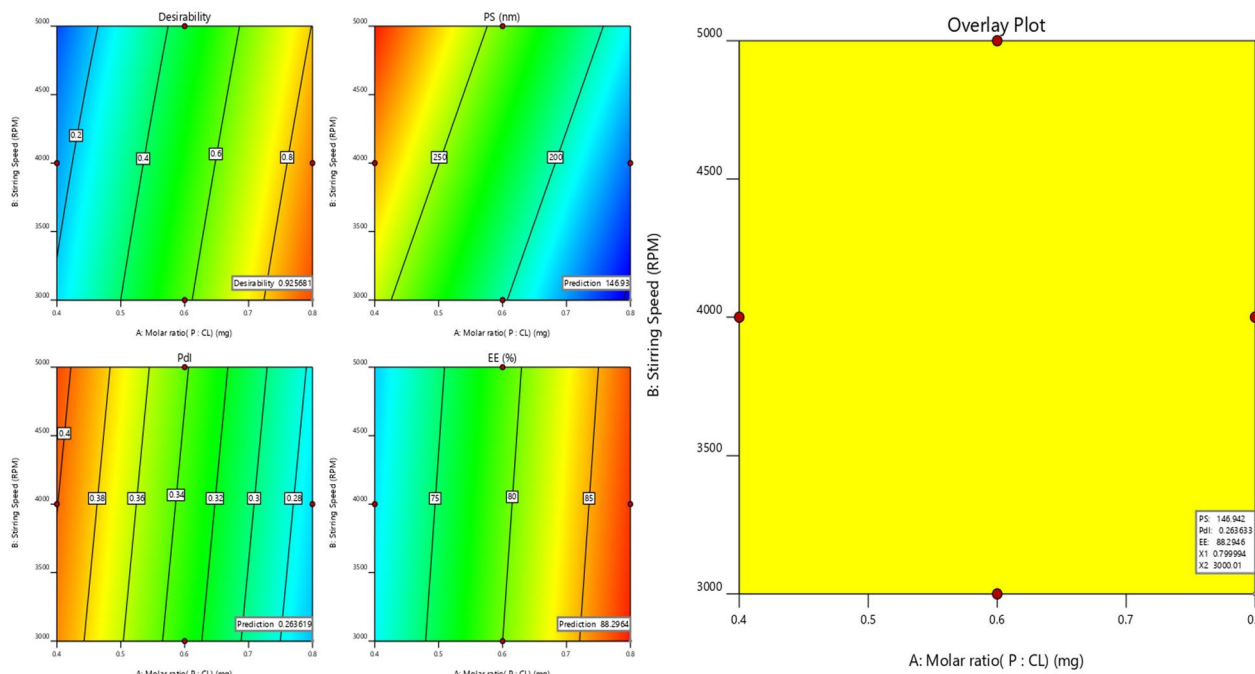


**Fig. 3** Graphical illustration of desirability plot as suggested by the design prediction and overlay plot (yellow area denotes the feasible region)



## EE

The impact of independent variables on EE ranges from 65.8 to 88.9 percent. Contour and surface response plots, as well as perturbation and Pred. versus actual plots for PS, Pdl, and EE, are depicted in Fig. 2. The model *F*-value of 42.62 indicates the suggested "linear" model's significance with negligible fit error. Lack of fit, statistically insignificant based only on pure error, yielded an *F*-value of 0.20. ANOVA identified significant factors (*p*-value < 0.0500), with non-significant variables removed to refine the model. Regression coefficient values ( $R^2$ , adjusted  $R^2$ , and anticipated  $R^2$ ) were 0.9208, 0.8992, and 0.8880, respectively. The model demonstrated utility in examining the design space, with an adequate precision (signal-to-noise ratio) of 18.68, exceeding the necessary value of 4. The model terms (*A*, *C*) were found to have *p*-values less than 0.050, indicating a substantial impact on the outcome. These terms are, therefore, considered required, and the regression equation that results is as follows:

$$\text{DrugEntrapment(DE)} = + 47.42A + 41.50A \\ - 0.0006B + 0.022C$$

A positive connection is indicated by the positive coefficients, which imply that a rise in the associated variable or variables causes an increase in entrapment of the drug [23].

## Exploration for optimized formulation

The design yielded solutions with desirability values, and the optimal formulation achieved a maximum attractiveness of 0.992. Optimum parameters included a stabilizer ratio of 0.8%, 2800-rpm stirring speed, and 395 min of stirring duration. These parameters effectively narrowed the target values of critical quality attributes (CQAs) for further graphical customization, as depicted in Fig. 3.

## Design confirmation

Three checkpoints were used to verify the model's robustness and formulation accuracy during validation. As indicated in Table 4, the projected mean standards for size, Pdl, and EE values were mentioned, while the

observed mean values were 150.3 nm, 0.281, and 86.76, respectively. The proposed model was validated by the close match between the software's anticipated values and the results achieved from these formulations (Table 4 and Fig. 4).

## Measurements of PS, Pdl, EE, and yield percentage

The produced formulation exhibited consistent particle sizes and nanosuspension uniformity, with PS ranging from  $151.8 \pm 5.6$  nm to Pdl of  $0.233 \pm 0.049$ . A Pdl value below 0.3 indicates a homogeneous system. Zeta potential measurement, indicative of colloidal particle surface charge, showed  $-17.3 \pm 2.26$  mV for the optimized formulation, suggesting stability due to steric stabilization by the stabilizer. Higher zeta potentials contribute to formulation stability. The entrapment efficiency (EE) and yield percentage for the optimized NSPs were  $87.36 \pm 1.61\%$  and  $56.57 \pm 2.09\%$ . Figure 4 illustrates PS, SEM images of pure drug, and optimized NSPs.

## Fourier transform infrared spectroscopy (FTIR), DSC, and XRD

The FTIR spectra of pure drug, physical mixture, blank HP $\beta$ CD NSPs, and drug-loaded HP $\beta$ CD D-NSPs are presented in Fig. 5. A scanning range of 400–4000  $\text{cm}^{-1}$  was used. The entrectinib drug exhibits characteristic peaks in its FTIR spectrum, indicating specific functional groups present. Peaks at 3344.68, 2923, and 2760  $\text{cm}^{-1}$  signify O–H and C–H stretching, while 1710  $\text{cm}^{-1}$  represents C=O stretching. Peaks at 1631, 1589, and 1462  $\text{cm}^{-1}$  correspond to C=C stretching and C–H bending, providing valuable molecular information for characterization. In the HP $\beta$ CD spectrum, vibrations related to saccharides were evident at approximately 3343  $\text{cm}^{-1}$ , 2924  $\text{cm}^{-1}$ , 1645  $\text{cm}^{-1}$ , and 1025  $\text{cm}^{-1}$ , corresponding to O–H bending, C–O, O–H stretching, and C–H stretching, respectively [24].

The  $\alpha$ -type glycosidic linkage showed a clear peak at 851  $\text{cm}^{-1}$ , suggesting the existence of glucopyranose units connected by  $\alpha$ -1, 4-glycosidic bonds. Peaks located at 2965  $\text{cm}^{-1}$  and 1365  $\text{cm}^{-1}$  were attributed to the anti-symmetric vibration and methyl peak in the hydroxypropyl group of HP $\beta$ CD. The spectrum of the physical blend of ENT and HP $\beta$ CD exhibited a merging of their individual peaks, suggesting the existence

**Table 4** Validation results

Solution 1 of 78 response	Predicted mean	Predicted median	Observed	Std. Dev	SE mean	95% CI low for mean	95% CI high for mean	95% TI low for 99% Pop	95% TI high for 99% Pop
PS	146.93	146.93	150.3	20.1512	13.3919	117.455	176.406	42.3925	251.468
Pdl	0.263619	0.263619	0.281	0.0324268	0.0215499	0.216188	0.31105	0.0953993	0.431838
EE	88.2964	88.2964	88.0	2.14317	1.42428	85.1616	91.4312	77.1784	99.4144

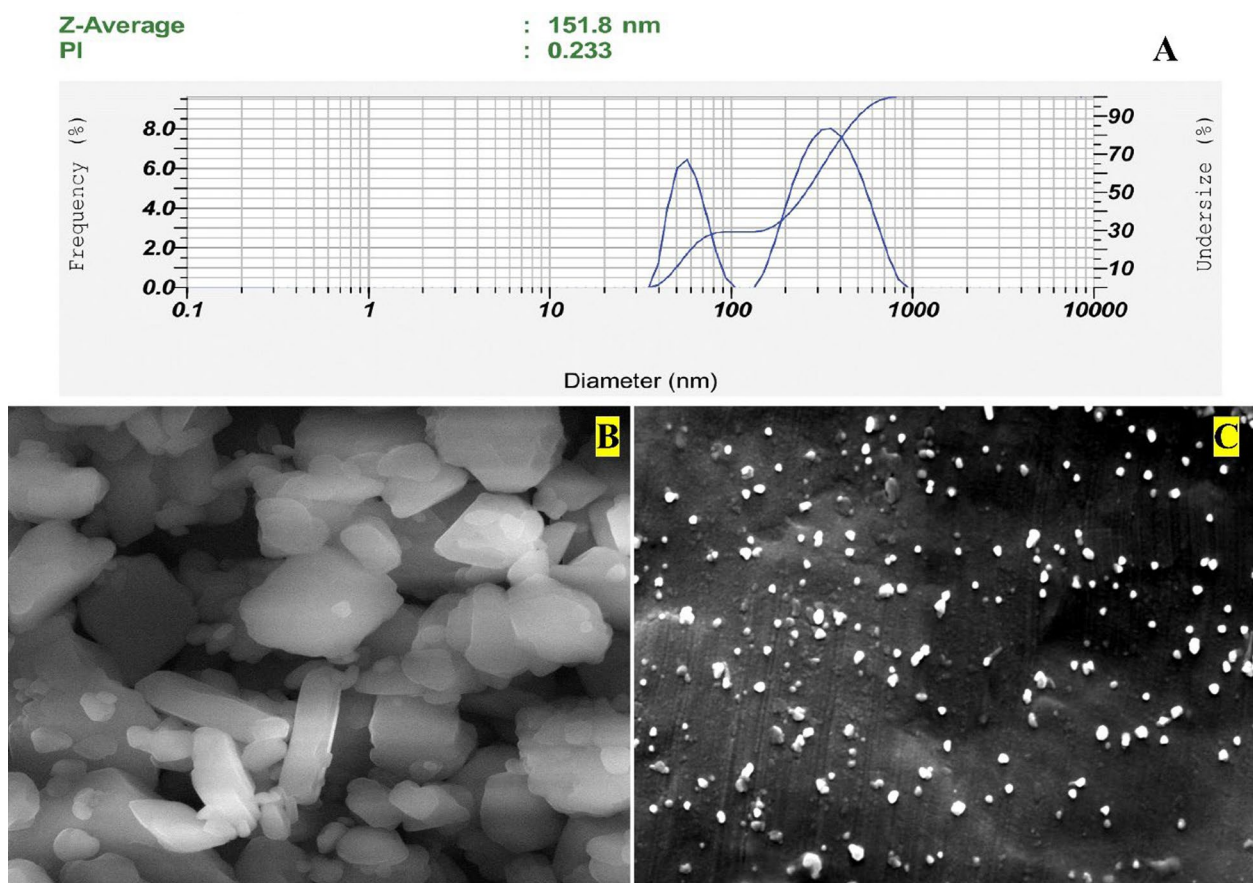


**Fig. 4** A Particle size (PS) and Pdl of the optimized nanosponges B SEM image of pure drug and C SEM image of the optimized NSPs

of distinctive peaks from both compounds. Notably, ENT's characteristic peaks were obscured by the nanosponge, suggesting potential bond reinforcement due to nanosponge–ENT interaction. Additionally, the O–H stretching vibration of ENT-HP $\beta$ CD transitioned to higher wavenumbers, suggesting the potential for hydrogen bond formation between the drug and HP $\beta$ CD.

The results of the DSC and XRD are shown in Fig. 5 B and C. The DSC analysis displays the melting behavior of an optimized ENT-NS, a physical mixture, and the pure drug. The drug demonstrated a melting endotherm, commencing at 206.23 °C, reaching its peak at 208.83 °C, and concluding at 211.71 °C. Conversely, HP $\beta$ CD exhibited a distinct melting behavior, commencing at a higher temperature of 251.11 °C, reaching its peak at 242.01 °C, and concluding at a significantly higher temperature of 277.98 °C. The plain drug is showing high intensity of peak as compared to nanosponges which can be attributed to the formation of inclusion complexes between entrectinib and HP $\beta$ CD [24].

#### Drug release (DR)

The drug release (DR) study, depicted in Fig. 6, compares the release profiles of ENT-loaded HP $\beta$ CD NSPs, pure ENT, and ENT-loaded HP $\beta$ CD complexes over time. ENT/HP $\beta$ CD complexes showed a rapid burst release, with over 95% released within 30 min and complete release within 2 h. In contrast, optimized HP $\beta$ CD NSPs exhibit sustained release ( $84.48 \pm 6.88\%$ ) after 72 h, contrasting with plain drug release ( $31.26 \pm 5.55\%$ ). Regression coefficients for Korsmeyer–Peppas (0.9882) and Higuchi (0.9915) models suggest strong correlations, while lower coefficients are observed for zero-order (0.8927) and first-order (0.4906) models, implying constant rate and exponential decay, respectively [20].

#### Stability studies

Stability studies of ENT-loaded HP $\beta$ CD NSPs were conducted over 3 months at three different temperatures (Table 5). Particle size increased gradually over time at each temperature, ranging from  $150.3 \pm 4.3$  nm on the 1st day to  $162.22 \pm 5.80$  nm on the 3rd month at  $5 \pm 3$  °C, and to  $178.22 \pm 5.80$  nm at  $40 \pm 2$  °C. Pdl values remained

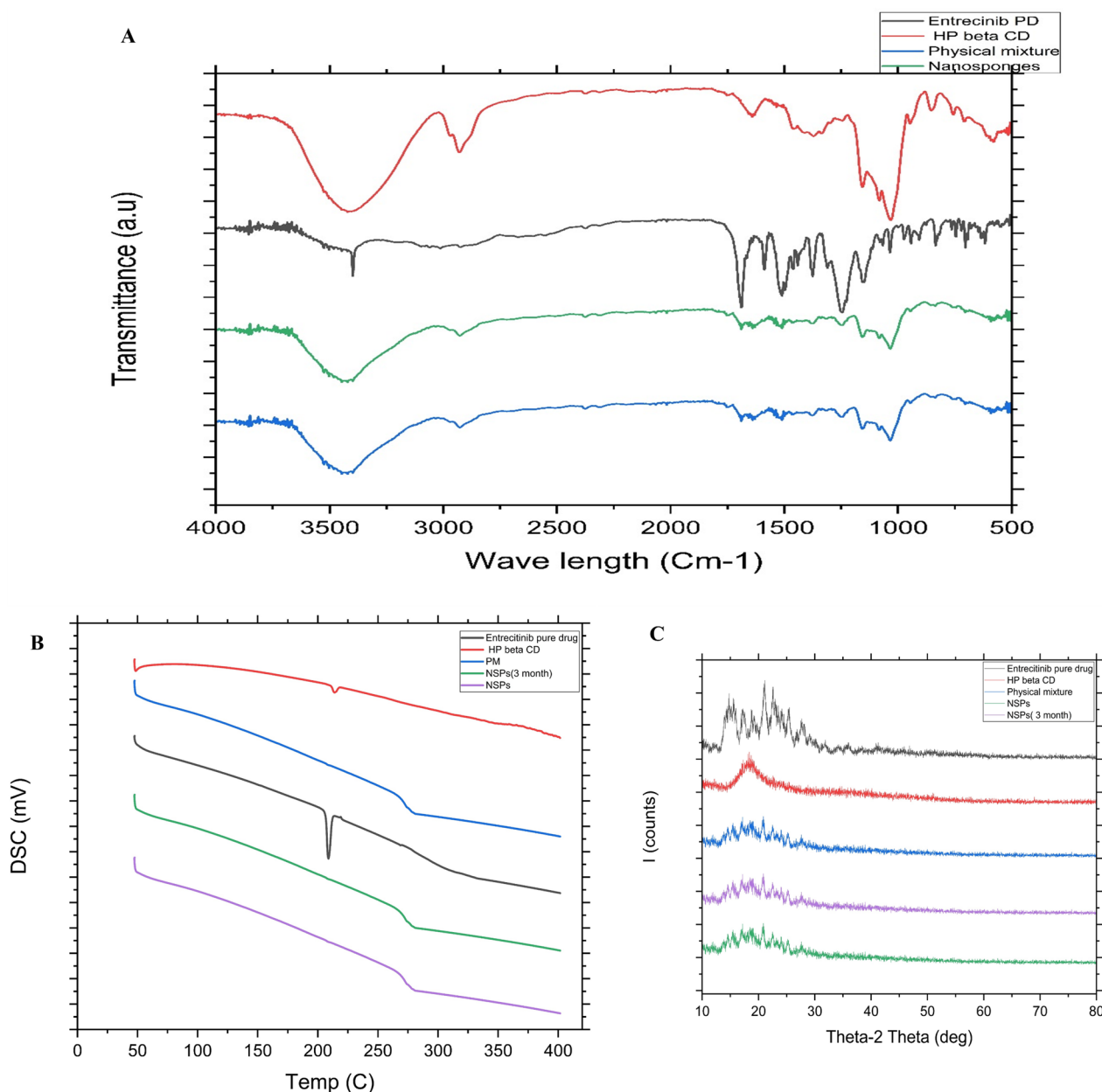


**Fig. 5** **A** Overlay FTIR spectra of **a** pure drug (black line); **b** physical mixture (blue line); **c** blank HPβCD NSPs (red line); and **d** drug-loaded HPβCD D-NSPs (green line). **B** Overlay of DSC thermograms of **a** entrecitinib pure drug (black line); **b** HPβCD (red line); **c** PM (physical mixture—blue line); **d** nanosponges–NSPs 3 months (green line); **e** nanosponges –NSPs (purple line). **C** Overlay of DSC thermograms of **a** entrecitinib pure drug (black line); **b** HPβCD (red line); **c** physical mixture (blue line); **d** nanosponges–NSPs (green line); and **e** nanosponges–NSPs 3 months (purple line)

relatively consistent over the duration of the study at all temperatures, indicating a uniform particle size distribution. However, EE values exhibited a decreasing trend over time at all temperatures.

**Kinetic studies**

Figure 7 displays the plasma concentration–time curve after administration of ENT in 0.25% w/v sodium

carboxymethylcellulose solution and the optimized nanosponges orally. Pharmacokinetic data in Table 6 reveal that the improved NSPs formulation exhibited significantly higher Tmax, Cmax (\*\*p < 0.001), AUC0-24 (\*\*p < 0.001), and AUC0-∞ (\*\*p < 0.001) values compared to the pure ENT suspension at the prescribed dose. The bioanalytical chromatogram indicated drug retention time at 5.52 min and internal standard (carbamazepine)

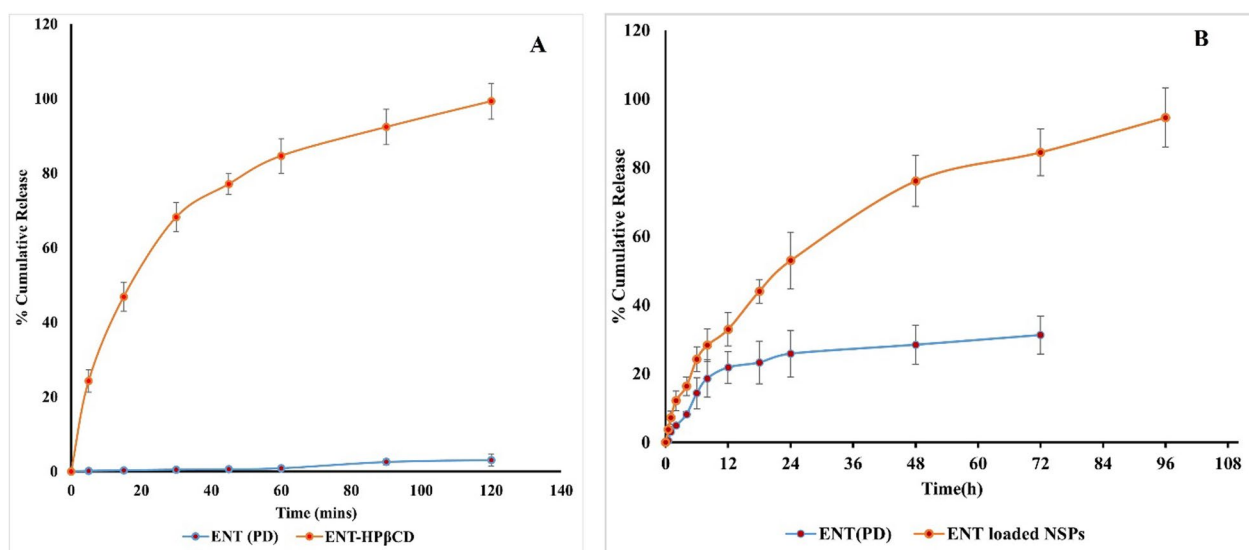


**Fig. 6** In vitro DR **A** ENT (PD) and ENT-HPβCD; **B** ENT (PD) and ENT-loaded NSPs

**Table 5** Short-term stability assessment of NSPs formulation: PS, Pdl, and EE analysis

Temperature	Months	PS (nm)	Pdl	EE (%)
5 ± 3 °C	Initial	150.3 ± 4.3	0.281 ± 0.020	88.29 ± 1.92
	0.5	150.8 ± 4.1	0.282 ± 0.022	88.00 ± 1.99
	1	152.6 ± 4.64	0.284 ± 0.032	87.42 ± 1.24
	2	156.08 ± 5.26	0.288 ± 0.021	87.48 ± 1.85
	3	162.22 ± 5.80	0.298 ± 0.024	86.02 ± 2.11
25 ± 2 °C	Initial	150.3 ± 4.3	0.281 ± 0.020	88.29 ± 1.92
	0.5	153.16 ± 3.65	0.285 ± 0.023	87.26 ± 2.33
	1	156.60 ± 4.42	0.288 ± 0.039	87.80 ± 3.41
	2	159.84 ± 6.02	0.292 ± 0.034	87.10 ± 4.68
	3	164.78 ± 4.04	0.298 ± 0.022	86.22 ± 3.89
40 ± 2 °C	Initial	150.3 ± 4.3	0.281 ± 0.020	88.29 ± 1.92
	0.5	156.61 ± 4.46	0.266 ± 0.032	87.01 ± 2.17
	1	162.05 ± 6.22	0.292 ± 0.033	86.36 ± 3.05
	2	169.04 ± 6.04	0.298 ± 0.020	85.49 ± 4.58
	3	178.22 ± 5.80	0.302 ± 0.021	83.56 ± 3.92

at 7.49 min (Suppl. Figure 2). NSPs showed a 4.10-fold increase in  $C_{max}$  and a 6.30-fold increase in  $AUC_{0-t}$  compared to the free drug.

## Discussion

In the current study, we formulated ENT-loaded HPβCD NSPs using an ultrasound-assisted technique. The Higuchi–Connors method was employed to determine the phase solubility profile, which demonstrated the creation of AL-type complexes between entrectinib (ENT) and

hydroxypropyl-β-cyclodextrin (HPβCD) [25]. HPβCD significantly enhances ENT's solubility in water, surpassing the solubility achievable with organic solvents typically used in pharmaceutical formulations. The interaction between HPβCD and ENT boosts the drug's water solubility, particularly at a saturated HPβCD concentration of around 40 mM. The nanosponge structure is maintained through hydrophobic interactions between the drug and HPβCD, while HPβCD's hydrophilic exterior enables dispersion of the nanosponges in water-based solutions. This advancement in solubility and stability expands the potential pharmaceutical applications of ENT [26].

BBD optimization resulted in a linear model for PS, Pdl, and EE. Positive coefficients indicate a rise in entrapment with increased variables. Higher and lower stabilizer concentrations led to increased particle sizes due to uncontrolled nuclei diffusion at lower concentrations. Despite acceptable Pdl values (<0.3), higher stirring rates caused a minor rise in Pdl due to increased particle energy, reducing repulsive forces and causing agglomeration, surpassing ideal homogenization. From the FTIR, it is clearly seen that ENT was masked by the HPβCD nanosponge, suggesting a potential reinforcement of bonds due to the interaction between the nanosponge and ENT. Additionally, the O–H stretching vibration of ENT-HPβCD experienced a displacement toward higher wavenumbers, suggesting the possible establishment of hydrogen bonds between the drug and HPβCD [24]. When entangled with cyclodextrin, the drug's melting point aligns with that of cyclodextrin, indicating robust interaction. In optimized drug-loaded HPβCD NSPs,

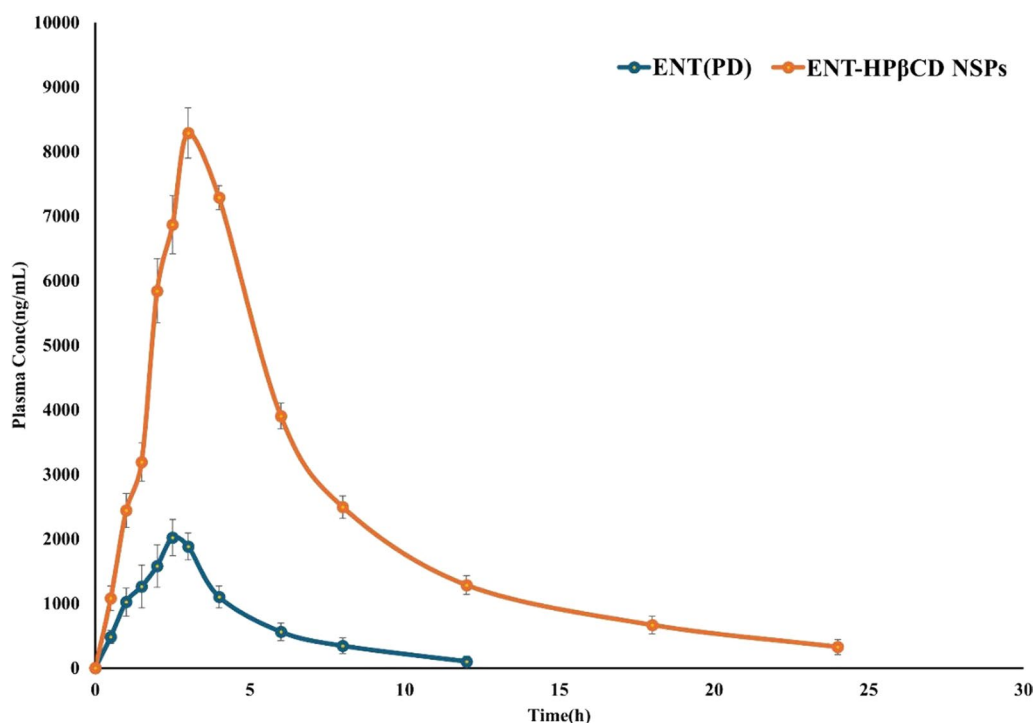


**Fig. 7** In vivo pharmacokinetic studies

**Table 6** Pharmacokinetic parameters

Pharmacokinetic parameters	ENT (PD)	ENT-loaded HPβCD NSPs
$C_{max}$ (ng/mL)	2021.52 ± 148.12	8290.66 ± 492.66
$T_{max}$ (h)	2.5	3
Half-life (h)	2.35 ± 0.39	6.079 ± 0.84
AUC 0-t (ng h/mL)	8914.38 ± 302.44	53,587.32 ± 422.06
AUC 0-inf (ng h/mL)	8960.42 ± 384.10	56,459.78 ± 462.31
$K_e$ (h <sup>-1</sup> )	0.294	0.114

drug entrapment within cyclodextrins signifies heightened thermal stability. The Kelvin effect further elucidates that isolated microscopic particles melt at lower temperatures than bulk. HPβCD molecules exhibit spherical aggregates and diverse solid-state forms, lacking a porous structure [27]. However, as seen in SEM pictures, these molecules combine to produce striking spherical morphologies with apparent porosity. Enclosure of entrectinib within HPβCD disrupts its crystalline structure, evident by decreased XRD peak intensity. This suggests entrectinib disperses or becomes amorphous within HPβCD, reducing sample crystallinity. Successful encapsulation within HPβCD nanospheres forms inclusion complexes, indicated by lower intensity XRD peaks. Burst pattern release from these complexes aligns with

prior studies, suggesting facile drug release through dilution or competitive complexation [25, 26].

On the other hand, the controlled release of ENT from nanospheres demonstrates a continuous pattern with no sudden burst effect, indicating the lack of loosely bound or unbound ENT on the HPβCD NSPs surface. The extended release behavior can be ascribed to the porous structure of HPβCD NSPs, which creates robust complexes with ENT, thereby averting any sudden release [26].

The incorporation of DPC in the structure of HPβCD NSPs enhances the ability of cyclodextrins to create complexes with guest molecules, thereby facilitating controlled release of drugs either by tight binding or regulated release mechanisms. This advancement holds potential for cancer treatment [28]. The regression coefficients imply a release mechanism combining diffusion (Higuchi model) and anomalous transport (Korsmeyer–Peppas model), indicating both matrix diffusion and polymer relaxation, swelling, or erosion contribute to drug release [29].

The ENT plasma nanospheres formulation showed a significantly higher area under the curve levels than those treated with pure drug. HPβCD NSPs formulation exhibits sustained release performance by supporting extended retention and improving bioavailability. The formulation's sustained release effect on ENT is confirmed by the longer half-life of the ENT-loaded



HP $\beta$ CD NSPs compared to the ENT suspension [30, 31]. Nonetheless, the pure drug suspension required less time to achieve the maximum plasma concentration (C<sub>max</sub>) than the optimized NSPs formulation. The NSPs carriers help to increase ENTs solubility and release, which results in notable improvements in pharmacokinetics.

## Conclusion

This study focused on the development of ENT-loaded DPC-crosslinked HP $\beta$ CD NSPs to address the challenge of poor bioavailability and inadequate sustained release of ENT in cancer management. By optimizing the formulation parameters, the HP $\beta$ CD NSPs achieved desirable characteristics including size, Pdl, and EE which are crucial for effective drug delivery systems. These optimized NSPs demonstrated sustained release of ENT, as evidenced by *in vitro* release studies, and enhanced bioavailability, as confirmed by *in vivo* pharmacokinetic evaluations. The porous nanoscale structure of the HP $\beta$ CD NSPs played a pivotal role in facilitating sustained drug release, ensuring prolonged therapeutic effect and improved efficacy compared to the pure drug formulation. Overall, these findings underscore the potential of optimized HP $\beta$ CD NSPs as a promising delivery system for cancer treatment, offering enhanced drug bioavailability and sustained release, which are crucial for effective management of cancer.

## Abbreviations

ENT	Entrectinib
HP $\beta$ CD	Hydroxypropyl-beta-cyclodextrins
NSPs	Nanosponges
PS	Particle size
Pdl	Polydispersity index
EE	Entrapment efficiency
FTIR	Fourier transform infrared spectroscopy
DSC	Differential scanning calorimetry

## Supplementary Information

The online version contains supplementary material available at <https://doi.org/10.1186/s43094-024-00680-8>.

Additional file 1.

## Acknowledgements

None.

## Author contributions

All the authors contributed equally.

## Funding

The authors did not receive any fund.

## Availability of data and materials

Upon request will provide the data.

## Declarations

### Ethics approval and consent to participate

The Institutional Animal Ethics Committee (IAEC) officially sanctioned the protocols designated by the assigned protocol number: 1447/PO/Re/S/11/CPCSEA-83/A.

### Competing interests

None.

### Author details

<sup>1</sup>Bir Tikandrajit University, Canchipur, Imphal West 795003, Manipur, India.

<sup>2</sup>Teegala Ram Reddy College of Pharmacy, Saroornagar (M), R R Dist, Meerpet, Hyderabad 500097, Telangana, India.

Received: 4 April 2024 Accepted: 3 August 2024

Published online: 14 August 2024

## References

- Rolfo C, Ruiz R, Giovannetti E, Gil-Bazo I, Russo A, Passiglia F, Giallombardo M, Peeters M, Raez L (2015) Entrectinib: a potent new TRK, ROS1, and ALK inhibitor. *Expert Opin Investig Drugs* 24:1493–1500. <https://doi.org/10.1517/13543784.2015.1096344>
- Rybarczyk-Kasiuchnicz A, Ramlau R, Stencel K (2021) Treatment of brain metastases of non-small cell lung carcinoma. *Int J Mol Sci* 22:1–21. <https://doi.org/10.3390/ijms22020593>
- Menichincheri M, Ardini E, Magnaghi P, Avanzi N, Banfi P, Bossi R, Buffa L, Canevari G, Ceriani L, Colombo M, Corti L, Donati D, Fasolini M, Felder E, Fiorelli C, Fiorentini F, Galvani A, Isacchi A, Borgia AL, Marchionni C, Nesi M, Orrenius C, Panzeri A, Pesenti E, Rusconi L, Saccardo MB, Vanotti E, Perone E, Orsini P (2016) Discovery of entrectinib: a new 3-aminindazole as a potent anaplastic lymphoma kinase (ALK), c-ros oncogene 1 kinase (ROS1), and pan-tropomyosin receptor kinases (Pan-TRKs) inhibitor. *J Med Chem* 59:3392–3408. <https://doi.org/10.1021/acs.jmedchem.6b00064>
- Sigal D, Tartar M, Xavier M, Bao F, Foley P, Luo D, Christiansen J, Hornby Z, Maneval EC, Multani P (2017) Activity of entrectinib in a patient with the first reported NTRK fusion in neuroendocrine cancer. *JNCCN J Natl Compr Cancer Netw* 15:1317–1322. <https://doi.org/10.6004/jnccn.2017.7029>
- Meneses-Lorente G, Bentley D, Guerini E, Kowalski K, Chow-Maneval E, Yu L, Brink A, Djebli N, Mercier F, Buchheit V, Phipps A (2021) Characterization of the pharmacokinetics of entrectinib and its active M5 metabolite in healthy volunteers and patients with solid tumors. *Invest New Drugs* 39:803–811. <https://doi.org/10.1007/s10637-020-01047-5>
- Satapathy S, Patro CS (2022) Solid lipid nanoparticles for efficient oral delivery of tyrosine kinase inhibitors: a nano targeted cancer drug delivery. *Adv Pharm Bull* 1:298–308
- Rozlytrek | European Medicines Agency, (n.d.). <https://www.ema.europa.eu/en/medicines/human/EPAR/rozlytrek> (accessed March 8, 2024)
- Otsu Y, Kata Y, Takayasu H, Inoue S, Kaneko T (2022) Entrectinib-induced heart failure in a patient with metastatic lung adenocarcinoma: a case report. *Cureus* 14:1247–1252. <https://doi.org/10.7759/cureus.32174>
- Otsu Y, Kata Y, Takayasu H, Inoue S, Kaneko T (2022) Entrectinib-induced heart failure in a patient with metastatic lung adenocarcinoma: a case report. *Cureus*. <https://doi.org/10.7759/cureus.32174>
- Reddy MR, Gubbiyappa KS (2022) Development of optimized self nano emulsifying systems of entrectinib for enhanced dissolution. [https://www.researchgate.net/publication/362806796\\_Development\\_of\\_optimized\\_self\\_nano\\_emulsifying\\_systems\\_of\\_entrectinib\\_for\\_enhanced\\_dissolution](https://www.researchgate.net/publication/362806796_Development_of_optimized_self_nano_emulsifying_systems_of_entrectinib_for_enhanced_dissolution) (accessed March 8, 2024).
- Mamatha P, Bhikshapathi DVRN (2023) Development, characterization and evaluation of entrectinib nanosponges loaded tablets for oral delivery. *Int J App Pharm* 15:269–281
- Alghaith AF, Mahrous GM, Zidan DE, Alhakamy NA, Alamoudi AJ, Radwan AA (2021) Preparation, characterization, dissolution, and permeation of flibanserine – 2-HP- $\beta$ -cyclodextrin inclusion complexes. *Saudi Pharm J* 29:963–975. <https://doi.org/10.1016/j.jpsps.2021.07.019>

13. Brewster ME, Loftsson T (2007) Cyclodextrins as pharmaceutical solubilizers. *Adv Drug Deliv Rev* 59:645–666. <https://doi.org/10.1016/j.addr.2007.05.012>
14. Utzeri G, Matias PMC, Murtinho D, Valente AJM (2022) Cyclodextrin-based nanosponges: overview and opportunities. *Front Chem* 10:859406. <https://doi.org/10.3389/fchem.2022.859406>
15. Almutairi BK, Alshetaibi A, Alali AS, Ahmed MM, Anwer MK, Aboudzadeh MA (2021) Design of olmesartan medoxomil-loaded nanosponges for hypertension and lung cancer treatments. *Polymers (Basel)*. <https://doi.org/10.3390/polym13142272>
16. Hu Q, Fu X, Su Y, Wang Y, Gao S, Wang X, Xu Y, Yu C (2021) Enhanced oral bioavailability of koumine by complexation with hydroxypropyl- $\beta$ -cyclodextrin: preparation, optimization, ex vivo and in vivo characterization. *Drug Deliv* 28:2415–2426. <https://doi.org/10.1080/10717544.2021.1998248>
17. Dhakar NK, Caldera F, Bessone F, Cecone C, Pedrazzo AR, Cavalli R, Dianzani C, Trotta F (2019) Evaluation of solubility enhancement, antioxidant activity, and cytotoxicity studies of kynurenic acid loaded cyclodextrin nanosponge. *Carbohydr Polym* 224:115168
18. Aldawsari MF, Alhowail AH, Anwer MK, Ahmed MM (2023) Development of diphenyl carbonate-crosslinked cyclodextrin based nanosponges for oral delivery of baricitinib: formulation, characterization and pharmacokinetic studies. *Int J Nanomed* 18:2239–2251. <https://doi.org/10.2147/IJN.S405534>
19. Sharma K, Kadian V, Kumar A, Mahant S, Rao R (2022) Evaluation of solubility, photostability and antioxidant activity of ellagic acid cyclodextrin nanosponges fabricated by melt method and microwave-assisted synthesis. *J Food Sci Technol* 59:898–908. <https://doi.org/10.1007/s13197-021-05085-6>
20. Moin A, Roohi NKF, Rizvi SMD, Ashraf SA, Siddiqui AJ, Patel M, Ahmed SM, Gowda DV, Adnan M (2020) Design and formulation of polymeric nanosponge tablets with enhanced solubility for combination therapy. *RSC Adv* 10:34869–34884. <https://doi.org/10.1039/d0ra06611g>
21. Sengupta P, Chatterjee B, Tekade RK (2018) Current regulatory requirements and practical approaches for stability analysis of pharmaceutical products: a comprehensive review. *Int J Pharm* 543:328–344. <https://doi.org/10.1016/j.ijpharm.2018.04.007>
22. Danaei M, Dehghankhold M, Ataei S, Hasanzadeh Davarani F, Javanmard R, Dokhani A, Khorasani S, Mozafari MR (2018) Impact of particle size and polydispersity index on the clinical applications of lipidic nanocarrier systems. *Pharmaceutics* 10:57. <https://doi.org/10.3390/pharmaceutics10020057>
23. Rangaraj N, Pailla SR, Chowta P, Sampathi S (2019) Fabrication of ibrutinib nanosuspension by quality by design approach: intended for enhanced oral bioavailability and diminished fast fed variability. *AAPS PharmSciTech*. <https://doi.org/10.1208/s12249-019-1524-7>
24. Yuan C, Liu B, Liu H (2015) Characterization of hydroxypropyl- $\beta$ -cyclodextrins with different substitution patterns via FTIR, GC-MS, and TG-DTA. *Carbohydr Polym* 118:36–40. <https://doi.org/10.1016/j.carbpol.2014.10.070>
25. Saokham P, Muankaew C, Jansook P, Loftsson T (2018) Solubility of cyclodextrins and drug/cyclodextrin complexes. *Molecules* 23:1161. <https://doi.org/10.3390/molecules23051161>
26. Loftsson T (2021) Cyclodextrins in parenteral formulations. *J Pharm Sci* 110:654–664. <https://doi.org/10.1016/j.xphs.2020.10.026>
27. Peimanfard S, Zarrabi A, Trotta F, Matencio A, Cecone C, Caldera F (2022) Developing novel hydroxypropyl- $\beta$ -cyclodextrin-based nanosponges as carriers for anticancer hydrophobic agents: overcoming limitations of host-guest complexes in a comparative evaluation. *Pharmaceutics* 14:1059. <https://doi.org/10.3390/pharmaceutics14051059>
28. Clemente N, Argenziano M, Gigliotti CL, Ferrara B, Boggio E, Chiocchetti A, Caldera F, Trotta F, Benetti E, Annaratone L, Ribero S, Pizzimenti S, Barrera G, Dianzani U, Cavalli R, Dianzani C (2019) Paclitaxel-loaded nanosponges inhibit growth and angiogenesis in melanoma cell models. *Front Pharmacol*. <https://doi.org/10.3389/fphar.2019.00776>
29. Argenziano M, Gigliotti CL, Clemente N, Boggio E, Ferrara B, Trotta F, Pizzimenti S, Barrera G, Boldorini R, Bessone F, Dianzani U, Cavalli R, Dianzani C (2020) Improvement in the anti-tumor efficacy of doxorubicin nanosponges in in vitro and in mice bearing breast tumor models. *Cancers (Basel)*. <https://doi.org/10.3390/cancers12010162>
30. Zidan MF, Ibrahim HM, Afouna MI, Ibrahim EA (2018) In vitro and in vivo evaluation of cyclodextrin-based nanosponges for enhancing oral bioavailability of atorvastatin calcium. *Drug Dev Ind Pharm* 44:1243–1253. <https://doi.org/10.1080/03639045.2018.1442844>
31. Omar SM, Ibrahim F, Ismail A (2020) Formulation and evaluation of cyclodextrin-based nanosponges of griseofulvin as pediatric oral liquid dosage form for enhancing bioavailability and masking bitter taste. *Saudi Pharm J* 28:349–361. <https://doi.org/10.1016/j.jsps.2020.01.016>

## Publisher's Note

Springer Nature remains neutral with regard to jurisdictional claims in published maps and institutional affiliations.